Synthesis of novel heteroleptic delocalised cationic pyrazole gold complexes as potent HepG2 cytotoxic agents

Article (Accepted Version)

Dalton Transactions

COMMUNICATION

Synthesis of Novel Heteroleptic Delocalised Cationic Pyrazole Gold Complexes as Potent HepG2 Cytotoxic Agents

Received 00th January 20xx,
Accepted 00th January 20xx

DOI: 10.1039/x0xx00000x

www.rsc.org/

Fatai Afolabi,[a] Wided Souissi,[b] Guillaume Rivière, [a] Clément Lemaitre, [a] S. Mark Roe,[a] Neil Crickmore[b]* and Eddy M. E. Viseux[a]*

A new series of cationic gold(I) pyrazole complexes were prepared in excellent yields as their perchlorate salts. Results of cell viability assays show that these novel complexes have good cytotoxic properties against the human HepG2 cancer cell line. These complexes showed promising anti-cancer activities and to our knowledge, pyrazoles have never been tested against this cell line. The regioselectivity of the complexation is also discussed in regards to the substitution pattern of the pyrazoles.

Introduction

Significant efforts have been made to advance the field of new transition metal-based drugs, with significant breakthroughs in chemotherapy and other diseases.[1,2,3] Many organometallic drugs employ the ability of a metal to lose one or more electrons to form a soluble cationic complex in biological fluids and exacerbate their binding affinity as a cation with biological electron donors such as DNA and proteins.[4] Their targets can include carriers of vital molecules to body tissues or the provision of structural frameworks to the body. Metals are also embedded into catalytic proteins and facilitate various chemical reactions essential for life.[4] The synthesis of organometallic complexes for biological reasons attracts considerable interest due to their wide-ranging applications, such as amino acid synthesis.[5] Over the past two decades, interest has increased in the organogold complexes for their high medicinal activities. Their structural design with simple and potent ligands are key aspects of medicinal inorganic chemistry with uses targeting varied afflictions such as asthma, malaria, rheumatoid arthritis, HIV[6] and cancer.[7,8] Furthermore, gold complexes are an excellent prototype for the rational design and development of novel and effective anti-cancer agents.[9] The activity of gold(I) complexes stems from their ability to penetrate the mitochondria and subsequently bind to the selenocysteine residue in thioredoxin reductase (TrxR).[10] TrxR is an enzyme usually over-expressed in tumour cells and involved in the growth and apoptosis of the cell. This overexpression hinders the apoptotic pathways.[7] The specificity of gold for mitochondria in cancerous cells was shown to arise from their hyperpolarisation, resulting in increased drug uptake compared to healthy cells, as we previously demonstrated.[3 11]

We investigated the design flexibility provided by anti-cancer agents based on gold(I) and found that gold with an amide linkage exhibit substantial activity against mammalian breast cancer cells.[12] This discovery on the nature of the linkage to gold to retain substantial anti-cancer activity regardless of the structure of the ligands is crucial to outsmart cancer resistance and improve potency. Ligand design has since been focused on features that are complementing the gold apoptotic pathways against cancerous cells. We decided to investigate pyrazoles because of their high medicinal value.[13] They are important building blocks used in pharmaceutical and agrochemical industries.[14,15,16] Pyrazole is a special class of heterocyclic compound that can not only coordinate to enzymes (through van der Waals interactions) but also to metals, making them useful templates for the design of novel drugs.[13,17] Their motif is also present in many biologically active compounds.[18] The structure/activity relationship (SAR) of pyrazoles alone has been extensively investigated and they were found to bind to a variety of receptors, enhancing the activity of many anti-angiogenesis agents.[19] Pyrazoles have also shown great pro-apoptotic potential against lung cancer cell lines[20] as well as excellent cytotoxicity against cells carrying the p53 cancer mutation Y220C.[21] Pyrazolates and imidazolates substituted with deactivating groups were used to synthesise neutral azolate gold(I) phosphane complexes and were found to act as anti-cancer agents.[22] The choice of the substitution pattern was based on previous observations whereby substitution R^3 at the 4-position (scheme 1) seemed to stabilise binding to p53-Y220C

[a] Department of Chemistry, School of Life Sciences, University of Sussex, Brighton, BN1 9QJ, UK. E-mail: E.M.E.Viseux@sussex.ac.uk; Tel: +44 (0) 1273 678621
[b] Department of Biochemistry, School of Life Sciences, University of Sussex, Brighton, BN1 9QJ, UK. E-mail: N.Crickmore@sussex.ac.uk; Tel: +44 (0) 1273 678917

† Footnotes relating to the title and/or authors should appear here.
Electronic supplementary information (ESI) available: Experimental and crystallographic details, NMR spectra. CCDC 1854268 to 1854271. For ESI and crystallographic data in CIF or other electronic format see DOI: 10.1039/x0xx00000x

through London interactions in a lipophilic pocket.[21] Substitution at the N2-position and N1- positions A closer look at the X-ray diffraction of the protein shows further possible interactions, notably Debye and Keesom dipolar interactions with the carbonyl at P153 and P152. We decided to include a range of substitutive functional groups (pyridine, bromo-phenyl, nitrile and bromine) to verify any impacts of such interactions on the activity of our complexes. The inhibitory properties of neutral gold(I) triphenylphosphine complexes on *E. coli* dihydrofolate reductase was found to be toxic against different human cancer cell lines.[23]

In our search for dual action orthogonal drug and based on our previous observations of the reactivity of gold amide complexes on cancer cells,[12] we decided to investigate a different class of amide ligands that is known to be active against cancer cells, yet with a different pathway to that of gold(I) alone, to further the applicability of anticancer drug candidates based on a gold-nitrogen bond. We investigated in this paper the role of delocalised cationic gold pyrazole complexes against the HepG2 human liver cancer cell line. HepG2 is a cell line widely used as a model system for hepatocyte cancers. Hepatocellular carcinomas are notoriously difficult to treat due to the ease at which they develop resistance to most common chemotherapeutic drugs.[24]

Results and Discussion

Synthesis of the complexes

We herein report on the complexation of pyrazole ligands 1-5 to form an array of pyrazole gold(I) complexes 6-10 (Scheme 1, Table 1).

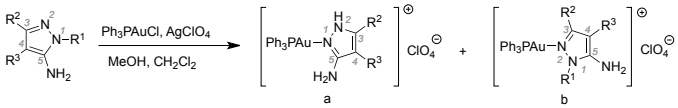

Scheme 1. Regioselective synthesis of pyrazole triphenylphosphinegold(I) perchlorates **6-10**.

The synthesis of these complexes is commonly hampered by long reaction times (two days and more)[25] and so our procedure was optimised to give rapid, facile and reproducible results. The successful synthesis of the intermediary cationic triphenylphosphinegold perchlorate was systematically assessed by ^{31}P NMR, and a single peak between 27 and 29 ppm, depending on the concentration, was observed. All complexes were characterised by ^{1}H, ^{13}C and ^{31}P NMR and their positive-ion ESI-MS displayed the $[M]^+$ peaks in agreement with the calculated isotopic pattern. Minor partial disproportionation to homoleptic complexes and to $[Au(PPh_3)_2]^+$ was observed for complex **6** (less than 0.1%) and for complex 9 (5%). Unfortunately, satisfactory crystals could not be grown for complex **6**, so its structure could not be ascertained. However, based on our observation for complexes where R^1 = H, it is highly probably that the regioselectivity should favour complex **6a** over **6b**. The results are collated in table 1.

Table 1: Synthesis of gold(I) pyrazole complexes.

Entry	R^1	R^2	R^3	Complex	Yield
1	H	H	Py	6	83%
2	H	H	Br-Ph	7a	94%
3	H	Methyl	Br-Ph	8a	88%
4	C_2H_4OH	H	CN	9b	95%
5	Methyl	H	Br	10b	87%

X-Ray diffraction

Suitable crystals for x-ray crystallography of complexes **7-10** were obtained by slow evaporation of dichloromethane and n-hexane in a [1:1] ratio although the crystals for complex **6** were too small for x-ray diffraction. The crystals were characterised by X-ray crystallography to confirm the atom connectivity and molecular geometry. The main results of the crystal structure determinations are reported in Table 2. Table 3 lists some selected bond lengths and angles of the four complexes.

Table 2. Crystal Data for complexes **7a**, **8a**, **9b** and **10b**

	7a	**8a**	**9b**	**10b**
Empirical formula	$C_{28}H_{25}N_3PBrAu$, ClO_4	$C_{27}H_{23}N_3PBrAu$, ClO_4	$C_{24}H_{23}N_4OPAu$, ClO_4	$C_{22}H_{21}N_3PBrAu$, ClO_4, CH_2Cl_2
Formula weight	810.80	796.78	710.85	819.64
Temperature/K	100.0(1)	173.0(1)	173.0(1)	173.0(1)
Crystal system	Triclinic	Orthorhombic	Triclinic	Monoclinic
Space group	P-1	Pbcn	P-1	$P2_1/c$
a/Å	12.7645(4)	18.9094(6)	13.2511(11)	13.8129(4)
b/Å	15.6061(5)	16.3880(5)	14.8189(13)	6.9184(2)
c/Å	16.4732(4)	17.9115(5)	15.7353(12)	29.6985(9)
α/°	105.959(2)	90	66.312(8)	90
β/°	93.268(2)	90	74.845(7)	103.268(3)
γ/°	112.402(3)	90	66.970(8)	90
Volume/Å^3	2868.22(16)	5550.6(3)	2584.0(4)	2762.33(14)
Z	4	8	4	4
ρ_{calc}/Mg/m^{-3}	1.878	1.907	1.827	1.971
μ/mm^{-1}	12.982	13.404	12.601	15.222
F(000)	1568.0	3072.0	1384.0	1576.0
Crystal size/mm	0.14 x 0.12 x 0.02	0.22 x 0.12 x 0.08	0.32 x 0.10 x 0.04	0.36 x 0.08 x 0.06
Reflections collected	31051	10573	15895	16828
Independent reflections/R(int)	10158/0.0544	5023/0.0393	9215/0.0310	5048/0.0394
Data/restraints/parameters	10158/60/707	5023/331/343	9215/8/671	5048/39/327
Goodness-of-fit[a] on F^2	1.093	1.057	1.022	1.151
Final R indexes [I>2σ(I)]	R_1[b]=0.0612, wR_2[c]= 0.1639	R_1[b]=0.0755, wR_2[c]= 0.2012	R_1[b]=0.0338, wR_2[c]= 0.0906	R_1[b]=0.0497, wR_2[c]= 0.1424
Largest diff. peak/hole/e Å^{-3}	5.17/-2.72	2.10/-1.10	1.25/-1.83	3.26/-1.29

a Goodness-of-fit = $[\Sigma(w(F_o^2 - F_c^2)^2]/(N_{obsevns} - N_{params})]^{1/2}$, based on all data.

b $R_1 = \Sigma(|F_o| - |F_c|)/\Sigma(|F_o|$, c $wR_2 = [\Sigma[w(F_o^2 - F_c^2)^2]/\Sigma[w(F_o^2)^2]]^{1/2}$.

Table 3. Selected bond lengths (Å) and angles (°) for complexes **7a**, **8a**, **9b** and **10b**

	7a	8a	9b	10b
Au – N1	2.048(7)		2.075(3), 2.055(4)	2.056(7)
Au – N2	2.042(6)	2.068(10)		
Au – P	2.238(2), 2.233(2)	2.241(3)	2.234(1), 2.223(1)	2.234(2)
N1 – N2	1.368(9), 1.374(8)	1.341(15)	1.368(5), 1.374(5)	1.367(11)
N1 – C5	1.337(10), 1.330(10)	1.317(16)	1.325(6), 1.333(6)	1.317(12)
N2 – C3	1.338(10), 1.355(9)	1.354(15)	1.351(6), 1.343(6)	1.357(12)
C3 – C4	1.393(11), 1.405(10)	1.382(16)	1.402(6), 1.407(6)	1.398(13)
C4 – C5	1.412(11), 1.396(11)	1.379(16)	1.384(6), 1.383(6)	1.395(13)
C3 – N6	1.393(10), 1.410(10)	1.327(17)	1.342(6), 1.337(6)	1.340(13)
C4 – C7	1.477(10), 1.470(11)	1.484(16)	1.419(6), 1.418(6)	
C4 – Br7				1.859(9)
P – C9	1.815(8), 1.817(7)	1.803(12)	1.812(4), 1.814(4)	1.812(9)
P – C10	1.818(8), 1.811(7)	1.805(12)	1.813(5), 1.801(5)	1.816(9)
P – C11	1.808(7), 1.816(7)	1.795(15)	1.819(4), 1.805(4)	1.813(9)
N1 – Au – P	176.68(19)		176.01(11), 176.98(11)	175.3(2)
N2 – Au – P	178.56(17)	175.3(3)		
Au – N1 – N2	123.3(5)		125.7(3), 125.1(3)	124.4(6)
Au – N2 – N1	123.4(5)	119.9(8)		
Au – N1 – C5	131.1(5)		125.7(3), 127.6(3)	125.5(6)
Au – N2 – C3	130.3(5)	133.0(9)		
Au – P – C9	116.4(3), 111.3(2)	109.8(4)	113.42(14), 109.91(14)	113.4(3)
Au – P – C10	112.7(2), 111.8(2)	114.5(4)	111.98(14), 113.82(16)	112.1(3)
Au – P – C11	109.3(2), 112.8(2)	113.1(4)	113.86(14), 113.15(14)	112.2(3)
N1 – N2 – C3	111.6(6), 105.6(6)	106.5(10)	110.4(3), 110.4(3)	110.3(8)
N2 – C3 – C4	107.5(7), 110.1(6)	109.3(10)	106.5(4), 106.4(3)	106.1(8)
C3 – C4 – C5	104.6(7), 104.9(6)	104.9(10)	105.8(4), 106.3(4)	106.2(8)
C4 – C5 – N1	110.7(7), 108.2(6)	108.8(11)	110.5(4), 109.8(4)	109.9(8)
C5 – N1 – N2	105.5(6), 111.1(6)	110.5(10)	106.8(3), 107.0(3)	107.4(8)
N2 – C3 – N6	120.8(7), 121.2(6)	120.7(12)	124.5(4), 124.0(4)	125.3(9)
N6 – C3 – C4	131.6(7), 128.7(7)	129.9(12)	128.9(4), 129.4(4)	128.3(9)
C3 – C4 – C7	129.2(7), 128.2(7)	126.2(10)	126.5(4), 126.6(4)	
C7 – C4 – C5	126.2(7), 126.9(7)	128.8(11)	127.6(4), 127.0(4)	
C3 – C4 – Br7				125.6(7)
Br7 – C4 – C5				128.2(7)
C4 – C5 – C8	129.6(7), 131.3(7)			
C8 – C5 – N1	119.6(7), 120.5(7)			

Figure 1 shows the structures in ORTEP format with the selected numbering scheme.

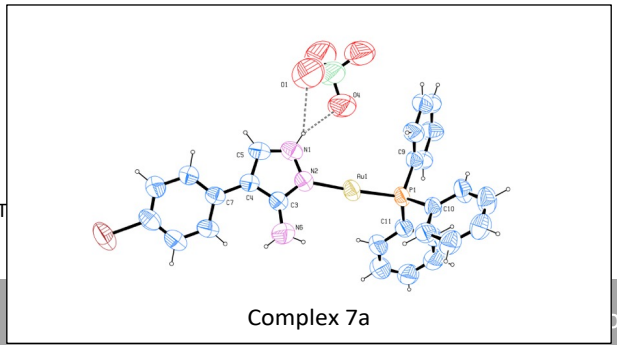

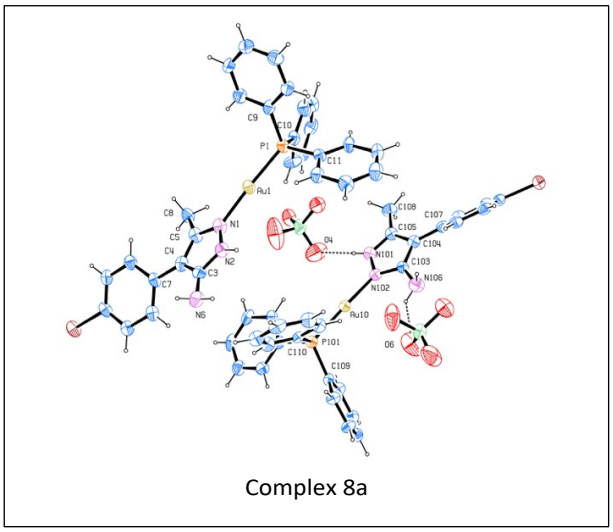

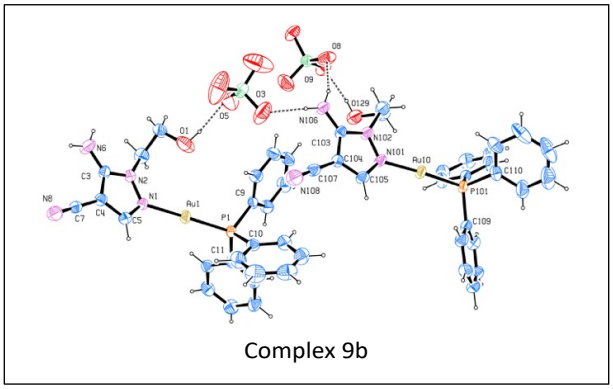

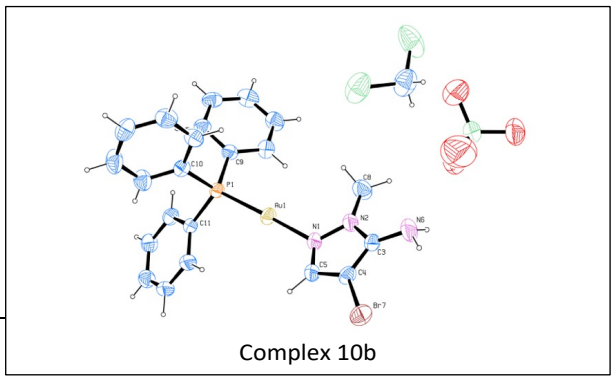

Figure 1. ORTEP views of complexes **7a**, **8a**, **9b** and **10b**, showing the numbering scheme used.

Selected crystalline specimens of the complexes **8a**, **9b** and **10b** were mounted on Mitegen loops and centered on the

goniometer head of a Rigaku Oxford Diffraction Gemini E diffractometer equipped with an EOS CCD area detector, data collection was performed at 173K. Complex **7a** was collected on a Rigaku Oxford Diffraction 007HFM/AFC11 diffractometer equipped with a Saturn 944+ CCD area detector at 100K. All complexes were collected with monochromated CuKα radiation, by means of ω-scans. The diffraction intensities were corrected with respect to Lorentz and polarization effects. Empirical multi-scan absorption corrections, using equivalent reflections, were also performed with the scaling algorithm SCALE3 ABSPACK. Raw data collection, data reduction and refinalisation were carried out with the CrysAlisPro software. All complexes were solved by means of the intrinsic phasing method in SHELXT[2623]and refined by full-matrix least squares methods based on F_o^2 with SHELXL[27]in the framework of the OLEX2[28]software. In the last cycles of refinement all non-hydrogen atoms were refined anisotropically; hydrogen atoms were placed and refined as riding atoms with their isotropic displacement parameters set to 1.2 times the U_{eq} of the parent atom. The best crystal of complex **7a** necessitated the collection on the Rigaku 007HFM due to its small size. In complex **8a**, there is a small amount of disorder relating to the ligand binding through N2 or N1. The amount of disorder was too low to model satisfactorily, so this has been left unmodelled. The molecular structures of all complexes contained a two-coordinate Au centre with expected Au-P (2.2-2.4Å) and Au- N (2.0-2.2Å) distances and linear coordination irrespective of the state of molecularity in the crystal (Table 3).[11] The Au-P were in very good agreement with 2.25 Å reported by Keter et al[29] and 2.26 Å results of Cambridge Structural Database (CSD).[29] The perchlorate molecule was included in the lattice of the complexes **7-10** and CH_2Cl_2 was present only in the lattice of complex **10b**. These display H-bonding to the NH_2 and the endocyclic NH when R^1=H. Ligand **1** has a pyridine at the fourth position, which provides another possible point of attachment compared to others. There is four possibilities for the point of attachment to gold (I). Therefore, four peaks were expected by ^{31}P NMR but only one peak at 30.0 ppm was observed indicating that there is only one possible linkage. Ligand **2** is a pyrazole with a bromophenyl at position 4 with three possible points of attachment but only one peak at 31.0 ppm was observed. X-ray crystallography also confirmed one linkage. The point of attachment was the nitrogen at the position one replacing the proton in that position but leaving a positive charge on the nitrogen ligand **3** has a similar structure to ligand **2** but with a methyl group at position three. Three points of attachment were also possible but the ^{31}P NMR indicated a single attachment point to gold (I) by given only one peak at 31.50 ppm. X-ray result also confirmed the single point of attachment but indicated that complex **8a** is a regioisomer with a positive charge on the nitrogen in position 1. Ligand **4** has a cyano group at position four and an ethyl alcohol at position two given different likely point of attachment. However, ^{31}P NMR of the complex gave a single peak at 29.7 ppm indicating a single point of attachment to gold (I). X-ray diffraction indicated that complex **9b** is a regioisomer with only one point of attachment to gold (I). Ligand **5** has a bromo substituent at position 4 and a methyl group at position one. ^{31}P NMR indicated only one point of attachment with a single peak at 30.0 ppm and attested to by the x-ray diffraction study. The point of attachment was at position 2. Complex **10b** is non regioisomeric.

Cell viability assays

The biological activity of the complexes were assessed after dilution in DMSO/H_2O (10% v/v) and addition to HepG2 cells. Assays were performed in 96-well plates using the Promega CellTiter-Blue assay as an endpoint method with a 2-hour incubation with the assay reagent. This assay measures cell viability and is based upon the ability of living cells to convert a redox dye (resazurin) into a fluorescent product (resorufin). Each well received 90 µL of cell suspension at a density of 22,500 cells per well and was cultured overnight (at 37 °C/5% CO_2 humidified air) before 10 µL of the test sample was added. The experiments were set up in triplicate. The mock control wells received 90 µL of cell suspension and 10 µL of the appropriate buffer (DMSO/H_2O). Wells that contained just 100 µL of cell culture medium served as background fluorescence controls. Fluorescent readings were taken using the GloMax-Multi Detection System (Promega).

The five complexes shown in Table 1 all indicated that they possessed reasonable activity against this cell line in a preliminary screen (data not shown). To confirm this activity various doses were then tested alongside their respective un-complexed ligands. Figure 2 shows that even at the lowest dose tested (20 µM) all of the complexes showed high activity. In contrast the free ligands showed no significant activity at the same concentrations. Due to the high level of activity observed, further dilutions were made and tested (Figure 3). These data indicate that complexes 7a, 8a, 9b and 10a remain highly toxic at 2 µM while 6 is significantly less toxic at this concentration. IC_{50} values were calculated as 1.75 µM (6), 0.19 µM (7b), 0.31 µM (8b), 0.13 µM (9a) and 0.23 µM (10a).

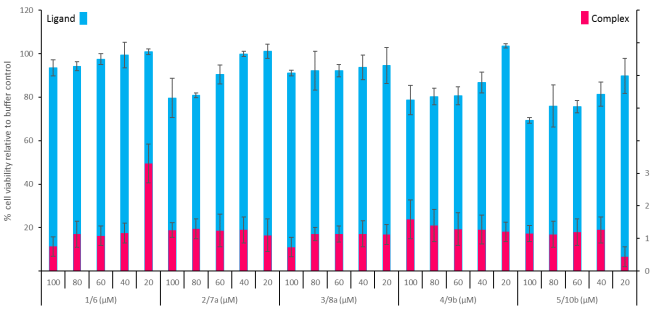

Figure 2. Toxicity data for the gold complexes (6-10 right hand scale) and their associated ligands (1-5 left hand scale) against HepG2 cells. Five doses of each compound were tested, background fluorescence was subtracted from each reading and the resulting values are shown relative to a buffer-only control (100% viability). Controls performed under full assay conditions confirmed that none of the compounds, or the separate ligands, interfered with the readings when tested at a concentration of 18 µM in the absence of cells. Error bars represent one standard error of the mean (SEM).

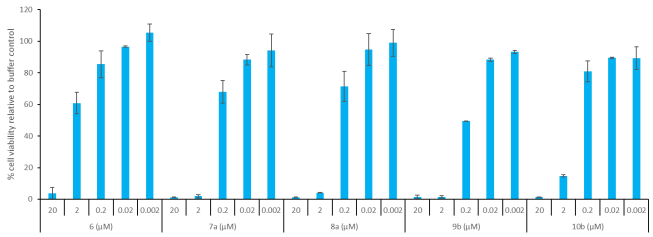

Figure 3. Dose response assay of gold complexes against HepG2 cells. Five doses of each complex were tested, background fluorescence was subtracted from each reading and the resulting values are shown relative to a buffer-only control (100% cell viability). Error bars represent one standard error of the mean (SEM).

Conclusions

Five new monocationic pyrazolium gold complexes **6-10** have been prepared in excellent yields and the substitution pattern did not seem to have a notable effect on their activity against the cancer cell line described herein. This flexibility in the design is desirable when fine tuning structural motifs for druggable applications. The regioselectivity of the complexation was found to be dependent on the substitution pattern on the endocyclic nitrogen N^1, favouring the complexation of the nitrogen proximal to the 5-amino group when R^1 = H. All compounds are highly active against HepG2 cancer cells and display activity in the submicromolar range comparable to our previous work on gold complexes and breast cancer cell lines.[3] Futhermore their efficacy compares well to other chemotherapeutic drugs on this cell line[30] including Doxorubicin (IC_{50} 1.1 μM) and Cisplatin (IC_{50} 15.9 μM) Hepatocellular carcinomas readily acquire resistance to chemotherapeutic drugs – usually through the expression of a multidrug efflux pump. It is unknown whether these mechanisms would prevent the action of our gold amides or whether they have potential in treating resistant cells. This work therefore provides strategic tools to investigate such avenues of research.

Acknowledgements

The authors wish to thank Dr Shane Lo Fan Hin for useful discussions, Prof. John Spencer for the provision of pyrazoles, Dr Iain Day for NMR spectroscopy, Dr Alaa Abdul Sada for Mass Spectroscopy and Prof. Michelle West for use of cell culture facilities.

Funding

The authors wish to thank the Tertiary Education Trust Funds (TETFund) of Nigeria and Osun State Polytechnic Iree, Osun State Nigeria for funding a PhD studentship (FA).

Conflicts of interest

The Authors declare that there are no competing interests associated with the manuscript.

Notes and references

1 N. Jaouen, G.; Metzler-Nolte, ed. N. Jaouen, G.; Metzler-Nolte, Springer, Berlin, 32nd edn., 2010.
2 E. Alesio, *Bioinorganic Medicinal Chemistry*, Weinheim, 2011.
3 S. Newcombe, M. Bobin, A. Shrikhande, C. Gallop, Y. Pace, H. Yong, R. Gates, S. Chaudhuri, M. Roe, E. Hoffmann and E. M. E. Viseux, *Org. Biomol. Chem.*, 2013, **11**, 3255–60.
4 C. Orvig and M. J. Abrams, *Chem. Rev.*, 1999, **99**, 2201–2204.
5 R. F. W. Jackson, *Recent Developments in the Application of Organometallic Chemistry to Amino Acid Synthesis*, American Chemical Society, Washington DC, ACS Sympos., 2009.
6 P. N. Fonteh, F. K. Keter and D. Meyer, *J. Inorg. Biochem.*, 2011, **105**, 1173–1180.
7 V. Gogvadze, S. Orrenius and B. Zhivotovsky, *Semin. Cancer Biol.*, 2009, **19**, 57–66.
8 K. Nomiya, R. Noguchi, K. Ohsawa and K. Tsuda, *J. Chem. Soc. Dalt. Trans.*, 1998, **2**, 4101–4108.
9 P. Gurunanjappa and A. K. Kariyappa, *Curr. Chem. Lett.*, 2016, **5**, 109–122.
10 I. Kostova and B. S. P. Bentham Science Publishers, *Anticancer. Agents Med. Chem.*, 2006, **6**, 19–32.
11 M. Bobin, I. J. Day, S. M. Roe and E. M. E. Viseux, *Dalton Trans.*, 2013, **42**, 6592–602.
12 S. Newcombe, M. Bobin, A. Shrikhande, C. Gallop, Y. Pace, H. Yong, R. Gates, S. Chaudhuri, M. Roe, E. Hoffmann and E. M. E. Viseux, *Org. Biomol. Chem.*, 2013, **11**, 3255.
13 D. Pal, S. Saha and S. Singh, *Int J Pharm Pharm Sci*, 2012, **4**, 98–104.
14 K. A. Kumar and M. Govindaraju, *Int.J. ChemTech Res*, 2015, **8**, 313–322.
15 T. S. Reddy, H. Kulhari, V. G. Reddy and V. Bansal, *Eur. J. Med. Chem.*, 2015, **101**, 790–805.
16 N. Hamada and N. Abdo, *Molecules*, 2015, **20**, 10468–10486.
17 A. Y. Shaw, H. Liau, P. Lu, C. Yang, C. Lee, J. Chen, Z. Xu and G. Flynn, *Bioorg. Med. Chem.*, 2010, **18**, 3270–3278.
18 H. Kumar, D. Saini, S. Jain and N. Jain, *Eur. J. Med. Chem.*, 2013, **70**, 248–258.
19 K. M. Kasiotis, E. N. Tzanetou and S. A. Haroutounian, *Front. Chem.*, 2014, **2**, 1–7.
20 G. M. Nitulescu, C. Draghici, O. T. Olaru, L. Matei, A. Ioana, L. D. Dragu and C. Bleotu, *Bioorg. Med. Chem.*, 2015, **23**, 5799–5808.
21 X. Liu, R. Wilcken, A. C. Joerger, I. S. Chuckowree, J. Amin, J. Spencer and A. R. Fersht, *Nucleic Acids Res.*, 2013, **41**, 6034–6044.

22 R. Galassi, A. Burini, S. Ricci, M. Pellei, M. P. Rigobello, A. Citta, A. Dolmella, V. Gandin and C. Marzano, *Dalt. Trans.*, 2012, **41**, 5307.
23 R. Galassi, C. S. Oumarou, A. Burini, A. Dolmella, D. Micozzi, S. Vincenzetti and S. Pucciarelli, *Dalt. Trans.*, 2015, **44**, 3043–3056.
24 A. X. Zhu, *Oncologist*, 2006, **11**, 790–800.
25 M. Munakata, S.-G. Yan, M. Maekawa, M. Akiyama and S. Kitagawa, *J. Chem. Soc. Dalt. Trans.*, 1997, 4257–4262.
26 G. M. Sheldrick, *Acta Crystallogr. Sect. A Found. Crystallogr.*, 2015, **71**, 3–8.
27 G. M. Sheldrick, *Acta Crystallogr. Sect. C Struct. Chem.*, 2015, **71**, 3–8.
28 O. V. Dolomanov, L. J. Bourhis, R. J. Gildea, J. A. K. Howard and H. Puschmann, *J. Appl. Crystallogr.*, 2009, **42**, 339–341.
29 F. K. Keter, I. A. Guzei, M. Nell, W. E. Van Zyl and J. Darkwa, *Inorg. Chem.*, 2014, **53**, 2058–2067.
30 F. Pascale, L. Bedouet, M. Baylatry, J. Namur and A. Laurent, *Anticancer Res.*, 2015, **35**, 6497–6504.

